ARTICLE
Journal of Cellular Biochemistry 115:697–711 (2014)

Journal of Cellular Biochemistry

Anticancer Bioactive Peptide-3 Inhibits Human Gastric Cancer Growth by Suppressing Gastric Cancer Stem Cells

Lan Yu,[1] Ling Yang,[2] Wei An,[1]* and Xiulan Su[1,2]**

[1]*Department of Cell Biology, Capital Medical University, No. 10 You An Men Wai Street, Fengtai District, Beijing 100069, China*

[2]*Clinical Medical Research Center of the Affiliated Hospital, Inner Mongolia Medical University, No. 1 Tongdao North Street, Huimin District, Hohhot 010050, China*

ABSTRACT

In the present study, the effective components of anticancer bioactive peptide-3 (ACBP-3), a novel antitumor agent isolated from goat liver, were analyzed. The CD44 (+) fraction of the human gastric cancer cell line was isolated, and the cells within this fraction that could form spheroid colonies (SCs) were identified as gastric cancer stem cells (GCSCs). Subsequently, the antitumor effect of ACBP-3 on GCSCs was investigated in vitro and in vivo. ACBP-3 dose-dependently decreased the percentage of CD44 (+) cells, suppressed the proliferation of the SC cells and inhibited their clone-forming capacity. Tumor formation from inoculated SC cells took substantially longer when the cells were treated with ACBP-3 in vivo. ACBP-3 alone or in combination with cisplatin suppressed xenograft tumor growth. The antitumor efficacy of cisplatin, when combined with ACBP-3, was enhanced even using half of the normal cisplatin dosage. The combination of cisplatin and ACBP-3 could partially alleviate the body weight loss in the mice. Moreover, treatment with ACBP-3 alone could prevent the body weight loss in the mice. Our study indicated that ACBP-3 inhibited gastric cancer cell growth by suppressing the proliferation of CSCs. ACBP-3 could be a potential CSC-targeting agent, and combined with cisplatin therapy, might be an effective way to clinically treat patients with cancer with a lower dose and reduced toxicity. J. Cell. Biochem. 115: 697–711, 2014.

KEY WORDS: ACBP-3; GASTRIC CANCER; CANCER STEM CELL; CD44; SPHEROID COLONY

Gastric cancer is the second most common cancer in males and the fourth most common cancer in females. More than 70% of new gastric cancer cases and deaths occur in developing countries, with the highest morbidity in eastern Asia [Jemal et al., 2011]. In China, the incidence of gastric cancer remains high, and many cases are commonly undiagnosed until the cancer has progressed to an advanced stage [Kamangar et al., 2006]. Poor prognosis and the propensity of relapse may be the main reasons for the low 5-year survival rate, approximately 20% [Nagini, 2012]. Much of the difficulty in treating this disease is due to the heterogeneity of the tumors, which include cancer cells with stem cell properties and more differentiated tumor cells. Cancer cells with stem cell properties are often referred to as cancer stem cells (CSCs) [Shiozawa et al., 2013]; these cells have altered cell cycle checkpoint control, potent chemotherapy- or radiotherapy-related DNA damage repair, impaired apoptosis machinery and upregulated multidrug resistance proteins [Signore et al., 2011]. Therefore, current therapies are mostly effective at eradicating non-CSCs rather than CSCs. The ability of CSCs to escape from radio- and chemotherapy are major hurdles to overcome in cancer treatment [Clarke et al., 2006; Saikawa et al., 2010]. A novel CSC-targeted therapy is urgently needed to treat gastric cancer patients.

Cisplatin is a metal-based antineoplastic drug that has been used extensively in the treatment of many cancers [Dickson et al., 2011]. In 2006, cisplatin was approved as one of the first line anti-cancer drugs for advanced gastroesophageal cancer in many countries [Ajani, 2008]. Its antineoplastic role is due to the DNA damage caused by the formation of platinum-DNA adducts, resulting in the activation of many signal transduction pathways [Prabhakaran et al., 2013]. However, cisplatin must be used at a very high dose to

The authors declare no conflicts of interests.

Grant sponsor: National Natural Science Foundation; Grant number: 81160254.

*Correspondence to: Wei An, Department of Cell Biology, Capital Medical University, 10 You An Men Wai Street, Fengtai District, Beijing 100069, China. E-mail: anwei@ccmu.edu.cn

**Correspondence to: Xiulan Su, Clinical Medical Research Center of the Affiliated Hospital, Inner Mongolia Medical University, 1 Tong Dao Street, Huimin District, Hohhot 010050, China. E-mail: xiulan139@163.com

Manuscript Received: 26 March 2013; Manuscript Accepted: 5 November 2013

Accepted manuscript online in Wiley Online Library (wileyonlinelibrary.com): 11 November 2013

DOI 10.1002/jcb.24711 • © 2013 Wiley Periodicals, Inc.

maximize its anti-cancer effect. Such an effective dose is impeded by its severe toxicities, including gastrointestinal toxicity, ototoxicity, peripheral neuropathy, and nephrotoxicity. Therefore, accumulating research has focused on developing a novel combination to achieve an enhanced efficacy with decreased side effects [El-Bialy and Rageh, 2013].

Anticancer bioactive peptide-3 (ACBP-3) is a polypeptide that was isolated from goat liver by our laboratory. In previous studies, we observed that ACBP-3 exhibited potent anticancer effects on human gastric cancer; more importantly, animals treated with this peptide exhibited few toxic effects during long-term experiments [Su et al., 2010]. In light of these traits, two major questions were raised: (1) is ACBP-3 able to suppress the gastric cancer stem cells (GCSCs), and if so, could it be used in CSC-targeted therapy and (2) if combined with cisplatin, could ACBP-3 attenuate the toxicity of cisplatin, reduce the effective dose, and enhance the efficacy of cisplatin? We aimed to answer the above questions by testing the anticancer effects of ACBP-3 in vitro and in vivo.

MATERIALS AND METHODS

ANALYSIS OF ACBP-3

ACBP-3 was prepared and purified as previously reported [Su et al., 2010]. ACBP-3 was analyzed using matrix-assisted laser desorption/ionization tandem time of flight mass spectrometry (MALDI-TOF/TOF-MS) (ultrafleXtreme; Bruker, Karlsruhe, Germany) and was separated using sodium dodecyl sulfate polyacrylamide gel electrophoresis (SDS–PAGE). The components obtained from the separation were further analyzed by MALDI-TOF/TOF-MS. The data were searched against the US National Center for Biotechnology Information (NCBI) database via the Mascot server (www.matrixscience.com).

CELL CULTURE

The human gastric cancer cell line MKN45 was purchased from the Cell Resource Center, Institute of Basic Medical Sciences, Chinese Academy of Medical Sciences, Peking Union Medical College (Beijing, China). The cells were cultured in RPMI 1640 culture medium (Invitrogen, Carlsbad, CA) supplemented with 10% fetal bovine serum (FBS; HyClone, Melbourne, Victoria, Australia) and 1% penicillin–streptomycin. After sorting, certain cells were cultured in serum-free medium supplemented with 10 mM HEPES, 20 ng/ml recombinant human epidermal growth factor (Invitrogen) and 10 ng/ml recombinant human fibroblast growth factor-basic (Invitrogen). All cells were maintained in a humidified 5% CO_2 incubator at 37°C.

FLOW CYTOMETRY ANALYSIS AND FLUORESCENCE-ACTIVATED CELL SORTING (FACS)

After the cells reached the logarithmic growth phase and were 70–80% confluent, they were washed twice with D-Hank's solution and digested with 0.05% trypsin-0.02% EDTA. After 9 min, culture medium was added to stop the digestion, and the mixture was centrifuged at 800 rpm for 5 min. The cell pellets were resuspended in phosphate-buffered saline (PBS) at a concentration of 1×10^7 cells/ml; then, 5 μl of mouse anti-human CD44 antibody (clone G44-26; BD Biosciences, San Diego, CA) labeled with fluorescein isothiocyanate (FITC) was added to 100 μl of the cell suspension. After incubation for 20 min on ice in the dark with interval mixing, the cells were centrifuged and washed two additional times with PBS, resuspended in PBS after the last wash, and analyzed or sorted using a flow cytometer (BD FACSAria; Becton, Dickinson and Company, Franklin Lakes, NJ). As a parallel control, the cultured cells were processed as above using a FITC mouse IgG2b k isotype control (clone 27–35; BD Biosciences). Unlabeled cultured cells served as a blank control.

To determine the effect of ACBP-3, the cells were treated with different doses of ACBP-3 for 48 h. Cells treated with normal saline (NS) served as the control. After labeling with CD44-FITC, the cells were rinsed in PBS and resuspended in 1 × binding buffer (Annexin V Apoptosis Detection Kit APC, Cat. 88-8007, eBioscience, San Diego, CA) at a density of 5×10^6 cells/ml. Five microliters of fluorochrome-conjugated Annexin V was added to 100 μl of the cell suspension and incubated at room temperature for 15 min. The cells were then washed in 1 × binding buffer and resuspended in 200 μl of 1 × binding buffer, followed by the addition of 5 μl of propidium iodide (PI) staining solution. Finally, the stained cells were immediately analyzed using flow cytometry.

SPHEROID COLONY (SC) FORMATION

The SC formation method has been the typical method for identifying CSCs in vitro. The ability of the candidate cells to form SCs in conditioned culture media is thought to represent the self-renewal ability [Liu et al., 2013]. Freshly FACS-sorted CD44 (+) and CD44 (−) cells were counted, and 5 CD44 (+) cells or 5 CD44 (−) cells were diluted in 200 μl of serum-free medium and inoculated into each well of an ultra-low attachment 96-well plate. The cells were examined weekly under a light microscope (Leica DM IL, Solms, Germany).

CLONE INHIBITION ASSAY

The SC-derived cells were selected and resuspended in complete culture medium or in complete culture medium containing 6 μg/ml ACBP-3. The cells were then cultured in 100-mm dishes at densities of 500, 1,000, or 2,000 cells per dish for approximately 14 days. When most of the cell clones in any of the dishes contained over 50–100 cells, the dishes were washed twice with PBS, fixed in 4% paraformaldehyde for 15 min, and dyed with Giemsa stain at room temperature for 30 min. After further washing with PBS to remove the excess dye, the culture dishes were air dried, and photos were taken. The assay was repeated three times to confirm the results.

INHIBITION OF CELL PROLIFERATION

The SC-derived cells were suspended in 100 μl of complete medium and inoculated into a 96-well plate at a density of 2×10^3 cells/well in sextuplicate. Twenty-four hours later, the cultures were treated with six different doses of ACBP-3, ranging from 10 to 25 μg/ml, or treated with NS, which served as the vehicle control. Untreated cells served as the blank control. After 24, 48, and 72 h, 20 μl of 5-(3-carboxymethoxyphenyl)-2-(4,5-dimethylthiazoly)-3-(4-sulfophenyl) tetrazolium, inner salt (MTS) reagent (Cat. number. G5421; Promega, Madison, WI) was added to the wells and incubated in a humidified, 5% CO_2 atmosphere at 37°C for 3 h. The absorbance at 490 nm was read using an ELISA plate reader (Biotek Instruments, Highland Park,

VT). The inhibiting rate (IR) of cell growth was calculated using the equation $(A - B)/A \times 100\%$, where A is the absorbance value of the blank control group, and B is the absorbance value of the experimental group or the vehicle control group.

APOPTOSIS ANALYSIS BY WESTERN BLOT

After 3×10^7 cells were treated with 22 μg/ml ACBP-3 for the indicated time and washed with PBS twice, the cells were harvested and lysed with 80 μl of lysis buffer [PBS, 0.15 M NaCl, 10 mM Hepes (pH 7.4), 1 mM EDTA, 1 mM EGTA, 1% Triton X-100 and 0.5% NP-40], supplemented with fresh protease inhibitor cocktail (Cat. 5871, Cell Signaling Technology). Sonication on ice for 10 s was used to lyse the cells. The lysate was incubated for 30 min on ice and centrifuged at 13,000 rpm 4°C for 10 min. The supernate was then collected, and the protein concentration was determined using a bicinchoninic acid (BCA). Protein Assay Kit (cat. 23225, Pierce, Rockford, IL). For each sample, 50 μg of the lysates, mixed with 5 × Laemmli buffer (1 M Tris-HCl pH 6.8, 50% glycerol, 10% SDS, 1% bromophenol blue, 10% β-mercaptoethanol), was denatured, subsequently cooled on ice, run on 12% SDS–PAGE and finally transferred onto PVDF membranes (Cat. LC2002, Invitrogen). The membranes were blocked with 5% BSA in Tris-buffered saline containing 0.05% Tween-20 (TBS-T) at room temperature for 1 h. Then, the membrane was briefly washed with TBS-T, incubated with the appropriate primary antibodies [anti-caspase-3 antibody (Cat. 9665) at a 1:1,000 dilution; anti-Bcl-2 antibody (human specific, Cat. 2872) at a 1:1,000 dilution; anti-Bax antibody (Cat.5023) at a 1:1,000 dilution, Cell Signaling Technology] at 4°C overnight. After further washing with TBS-T, the membranes were incubated with the corresponding secondary antibodies (1:7,000) for 2 h. The membranes were then developed using enhanced chemiluminescence (ECL) reagents.

CONFOCAL ANALYSIS OF F-ACTIN

After attachment, the cells were divided into two groups: one group was treated with 22 μg/ml ACBP-3 for 48 h, and the other group was incubated with NS, which served as a control. The cells were then fixed with fresh methanol-free 4% formaldehyde at room temperature for 15 min, washed with PBS and incubated with 0.3% Triton X-100 for 10 min. The cells were then stained with Alexa Fluor 555 Phalloidin (Cat. 8953, Cell Signaling Technology) at a 1:20 dilution for 30 min and rinsed once with PBS. These samples were examined using a Leica NT fluorescent confocal microscope (Leica, Wetzlar, Germany).

TUMORIGENICITY OF THE SC-DERIVED CELLS AND THE CD44 (−) CELLS

All animal experiments were conducted according to the Institutional Ethics Guidelines for Experimental Usage of Animals, Capital Medical University. The animals received humane care during the experiments. To confirm the tumorigenicity of the candidate cells, 8-week-old NOD/SCID female mice (Cancer Institute, the Chinese Academy of Medical Sciences, Beijing, China) were divided into two groups ($n = 6$ for each group). Three hundred SC-derived cells or 5×10^4 CD44 (−) cells were diluted in 0.1 ml PBS and were subcutaneously injected into the axillary regions of the mice. The mice from each group were monitored weekly for up to 10 weeks for xenograft tumor growth.

TUMORIGENICITY OF THE SC-DERIVED CELLS TREATED WITH ACBP-3

After confirming the tumorigenicity of the SC-derived cells, the effect of ACBP-3 on their tumorigenicity was examined. The SC-derived cells were incubated in culture medium for 12 h and were then divided into two groups. In the ACBP-3 group, the cultures were treated with 19 μg/ml ACBP-3 for 48 h; the control cells were treated with NS. Afterwards, the cells were labeled with fluorochrome-conjugated Annexin V and PI, followed by FACS. The healthy SC-derived cells that were both Annexin V negative and PI negative were collected and counted. Then, 3×10^4 healthy SC-derived cells from the ACBP-3 group were diluted in 0.1 ml of PBS and then grafted subcutaneously into the left axillary region of 8-week-old NOD/SCID mice as described above. A similar amount of SC-derived cells from the control group were grafted simultaneously into the right axillary region of the same mice. The mice were checked every 2 days for the presence of palpable tumors. Data from both injection sites were recorded continuously once the xenografts were palpable on either side. The mice were sacrificed at the end of the experiment when any mouse appeared moribund.

EFFECTS OF ACBP-3 ON HEALTHY MICE

Parallel to the above experiment, the toxicity of ACBP-3 in healthy animals (8-week-old BALB/C female mice, bought from the Animal Center, Chinese Academy of Military Sciences, Beijing, China) was investigated. The ACBP-3 mice ($n = 8$) were intraperitoneally injected with 31.3 μg of ACBP-3 per day, whereas the control mice ($n = 8$) received the same volume of NS. The body weight, feeding status and living status were observed every 2 days for 7 weeks.

XENOGRAFT MODEL AND TREATMENT

The inhibition of tumor growth by ACBP-3 was observed in tumor-bearing mice. As described above, 3×10^4 SC-derived cells from the MKN45 cell line were grafted into the mice. As a result, all of the mice developed single palpable tumors approximately 2 weeks later. Mice with a tumor volume smaller than 80 mm^3 or larger than 100 mm^3 or mice with tumor diabrosis were excluded from further experiments. The mice were injected via the caudal vein every 2 days, with 12.52 μg of ACBP-3, 0.2 mg of cisplatin or their combination (6.26 μg of ACBP-3 and 0.1 mg of cisplatin), each diluted in 200 μl of NS. A similar amount of NS was administered to mice as a control. The data were measured every 2 days. All of the mice were simultaneously sacrificed at the end of the experiment.

DETECTION OF TOTAL CYTOKERATIN 18 (CK18)

Plasma CK18 is a biochemical indicator of tumor necrosis. To evaluate the killing effect of ACBP-3 on the tumors, the levels of total CK18 were detected. Blood was withdrawn from the mice before and after drug interference. Before the administration of a drug, blood was taken carefully via a retro-orbital method. Upon the termination of experiment, the mice were sacrificed, and their blood was collected again. The plasma was immediately stored at −80°C. CK18 was measured in the samples of the mice taken before and after drug treatment.

For detection, 25 μl of plasma were added to each well of a 96-well plate in duplicate. Total CK18 was detected using the M65

ELISA (Cat No. 10020, Peviva, Bromma, Sweden), and the procedure was conducted strictly according to the manufacturer's instructions. The ELISA readouts were recorded. The relative ratio of total CK18 was calculated using (A/V)/(B/VN), where A is the readout of each sample, V is the corresponding mouse tumor volume, B is the readout of the NS group, and VN is the tumor volume of the NS group.

HE STAINING

The SC-derived cells were plated on sterile microscope coverslips coated with aminopropyltriethoxysilane (APES) in complete medium for 24 h. After adhesion, half of the cells were treated with 22 μg/ml ACBP-3 for another 48 h; the remaining cells remained untreated and were used as a control. After HE staining, the cell morphology was observed under a light microscope.

The tissues from the xenograft tumors were dissected after the mice were sacrificed. The tissues were fixed in 4% paraformaldehyde and embedded in paraffin. The sections were then prepared for HE staining.

SCANNING ELECTRON MICROSCOPY (SEM)

The SC-derived cells from the MKN45 cell line were treated with different doses of ACBP-3 (16 and 22 μg/ml) for 48 h after their adhesion to coverslips coated with poly-L-lysine, whereas the untreated SC-derived cells were used as a control. All of the cells were fixed in 2.5% glutaraldehyde in 0.1 M PBS (pH 7.4) at 4°C for 2 h, washed in PBS, and post fixed with 1% osmium tetraoxide in PBS. The cells were then dehydrated stepwise using a graded isoamyl acetate series and a hexamethyldisilazane process flow. Cell samples were viewed using a SEM (TM1000; Hitachi, Japan).

TRANSMISSION ELECTRON MICROSCOPY (TEM)

The SC-derived cells from the MKN45 cell line were incubated in 10-cm culture dishes for 24 h, processed with ACBP-3 as mentioned above, and harvested. These cells, or the freshly dissected tumor tissues from mice, were processed similar to the above-described procedure. After the propylene oxide process, the cell or tissue samples were embedded in epoxy resin, and ultrathin sections were stained with uranyl acetate/lead citrate and viewed using a TEM (H7650; Hitachi).

CD44 ANALYSIS BY IMMUNOHISTOCHEMISTRY

The tissue sections of the xenograft tumors were deparaffinized with xylene, rehydrated in a series of alcohols and incubated in 3% hydrogen peroxide at room temperature for 10 min to inactivate the endogenous peroxidase. Following incubation, the slides were rinsed three times with PBS. Antigen retrieval was performed according to common protocols. The slides were blocked with serum for 30 min to reduce the non-specific binding and were then incubated with CD44 antibody (Cat. 3570, Cell Signaling Technology) at a 1:50 dilution at 4°C overnight. The slides were then incubated with polyclonal goat anti-mouse IgG (biotinylated, product No. E043301, Dako, Glostrup, Denmark) at a 1:400 dilution at room temperature for 30 min, followed by incubation with labeled polymer-HRP (Code K4000, Dako) in a humid chamber at room temperature for 30 min. The signal was visualized using 3,3′diaminobenzidine (DAB) substrate (Code K4000, Dako). All sections were counterstained with hematoxylin, followed by dehydration and mounting.

The immunohistochemical staining was analyzed using the Leica Qwin Image Processing and Analysis Application. For each slide from the xenograft tumors subjected to different treatment, 8–10 snapshots were randomly chosen for counting; however, areas containing overt necrosis were unquantifiable and were avoided. The percentage of CD44 positive cells was calculated accordingly.

EXPERIMENTS EXTENDED TO AN ALTERNATIVE HUMAN GASTRIC CANCER CELL LINE

To further examine the effects of ACBP-3, an alternative gastric cancer cell line, MKN74, was used. This cell line was purchased from Riken (Ibaraki, Japan; http://www.brc.riken.go.jp/lab/cell/english). Similar experiments were conducted, and the relative methods, such as cell culture, flow cytometry, FACS, SC formation, tumorigenicity, cell growth and inhibition, were the same as those mentioned above.

STATISTICS

The data are presented as the mean values ± standard deviation (SD). Comparisons between groups were evaluated using a *t*-test; multiple comparisons were analyzed by one-way ANOVA. $P < 0.05$ was deemed statistically significant. All statistical tests were conducted using the computer software SPSS v.17.0 (SPSS, Inc., Chicago, IL).

RESULTS

ACBP-3 IS A MIXTURE MAINLY COMPOSED OF SIX PEPTIDES

ACBP-3 was analyzed by MALDI-TOF/TOF-MS. Eight main peaks (peak 1–8) based on mass spectrographic analysis were recorded, for which the maximal peak indicated the substance with the highest content in the mixture. The mass/charge (m/z) ratios of the peaks were within 4,084.299–14,343.103 (Fig. 1A). The mass spectrum displayed two substances with two spectral forms. For example, the $(M+2H)^{2+}$ form of one substance was located at peak 1, whereas its $(M+H)^{+}$ form had an m/z value of 8,444.524 (peak 6) (M: molecular weight; H: hydrogen atom; $^{+}$: positive charge). The m/z values of 7,158.395 and 14,343.103 corresponded to another substance (Fig. 1A, peak 4 and peak 8, respectively). The ACBP-3 portion was then separated by SDS–PAGE and found to be mainly composed of five to six peptides. The molecular weight (MW) of the main components ranged from 7 to 9 kDa (Fig. 1B). Next, these peptides were digested using trypsin and further analyzed by MALDI-TOF/TOF-MS (Supplemental Fig. S1), and the data were searched and compared based on the NCBI database. Three of the six components of ACBP-3 were identified—components I, II, III—and their main data, with the highest score in the NCBI database, are detailed in Table I. Component I, the highest content in the mixture, was an ubiquitin-like substance. As ubiquitin is highly conservative in eukaryotes, component I could also be ubiquitin, or alternatively, ubiquitin-40S ribosomal protein S27a-like. Component II was a fatty acid-binding protein, and component III was a serum albumin precursor. However, the other three components remain unknown.

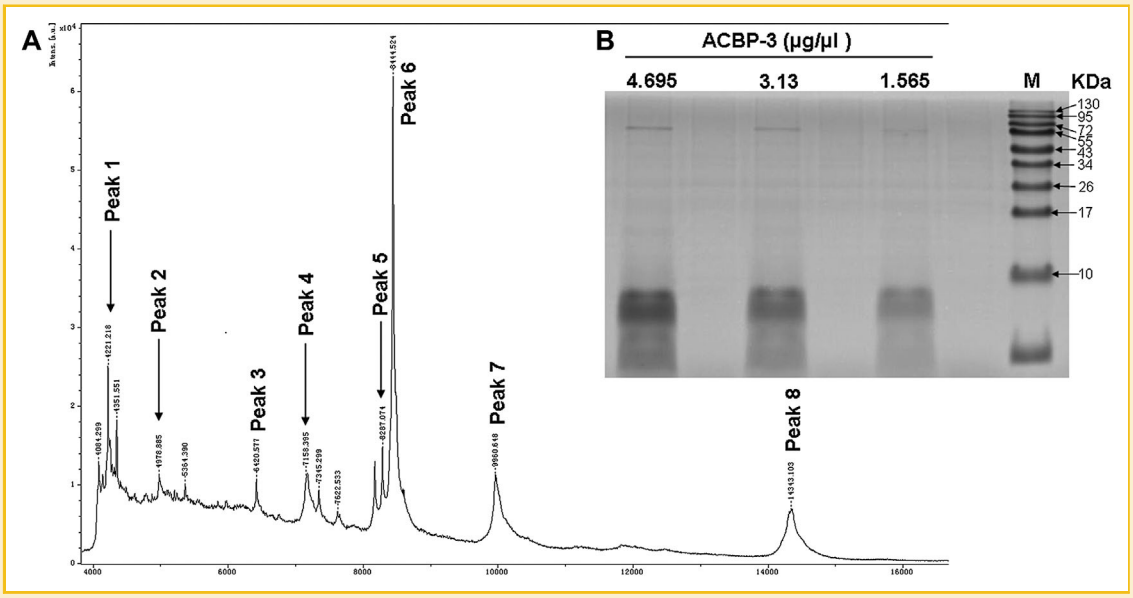

Fig. 1. Molecular characteristics of ACBP-3. A: Analysis of the components of ACBP-3 using MALDI-TOF/TOF-MS. The MW of the compositions varied. The $(M+2H)^{2+}$ form of one substance was located at the peak 1, whereas its $(M+H)^{+}$ form was located at peak 6; similar results were observed for peak 4 and peak 8. B: Gradually increasing concentrations of ACBP-3 were examined using 10% SDS-PAGE. M, marker.

CD44 (+) CELLS FROM THE MKN45 CELL LINE EXHIBITED SC FORMING ABILITY IN VITRO

A previous study confirmed that GCSCs were enriched in the CD44 (+) fraction of the gastric cancer cell line MKN45 [Takaishi et al., 2009]. To observe the effect of ACBP-3 on GCSCs, the candidate GCSCs needed to be identified first. Thus, we examined whether the CD44 (+) cells possessed the ability to form SCs. MKN45 cells derived from the 3rd or 4th passage were analyzed via flow cytometry, and the experiment was conducted five times. The percentage of CD44 (+) cells averaged 90.6% (Fig. 2A). Next, the ability to form SCs was assayed. CD44 (+) cells and CD44 (−) cells were cultured in serum-free medium after FACS, and the total inoculated cell numbers were 4,500 and 2,100, respectively. Cell viability was examined every week by Trypan blue staining. One week after inoculation, the CD44 (+) cells could not be stained, indicating that the cells were surviving. In contrast, approximately 20% of the CD44 (−) cells were Trypan blue positive (dead cells). At the 2-week point, most of the CD44 (−) cells appeared dead, whereas most of the CD44 (+) cells survived. After culture in serum-free media for 3–4 weeks under nonadherent conditions, some CD44 (+) cells were able to form SCs, and these SC-derived cells remained viable. At the 6th week, the SC-derived cells were still alive (Fig. 2B). For the CD44 (+) fraction, which was

TABLE I. Data of Identified Components of ACBP-3

	Matching number	Substance	Mass	Score	Sequences
Component I	gi 229532	ubiquitin	8,446	76	K.EGIPPDQQR.L K.ESTLHLVLR.L
	gi 148684097	mCG13235 [Mus musculus]	15,691	76	K.EGLPPDQQR.L K.ESTLHLVLR.L
	gi 159162145	Chain A, Rotamer strain as a determinant of protein structural specificity	8,560	76	K.EGIPPDQQR.L K.ESTIHLVLR.L
	gi 332213066	PREDICTED: ubiquitin-40S ribosomal protein S27a-like [Nomascus leucogenys]	18,240	76	K.EGIPPDKQR.L K.ESTLHLVLR.L
Component II	gi 28461261	Fatty acid-binding protein, liver [Bos taurus]	14,275	112	K.YQVQTQENYEAFMK.A
	gi 109103778	PREDICTED: fatty acid-binding protein, liver-like [Macaca mulatta]	9,844	50	K.YQLQSQENFESFMK.A
Component III	gi 1351907	Serum albumin precursor [Bos taurus]	71,244	110	K.LGEYGFQNALIVR.Y K.DAFLGSFLYEYSR.R

"Mass" indicates the mass value. "Score" indicates the scores marked via Mascot (www.matrixscience.com). "Sequence" indicates the amino acid sequence. "[Mus musculus], [Nomascus leucogenys], [Bos taurus], [Macaca mulatta]" indicates the homologous sequence from Mus musculus, Nomascus leucogenys, Bos Taurus, and Macaca mulatta, respectively.

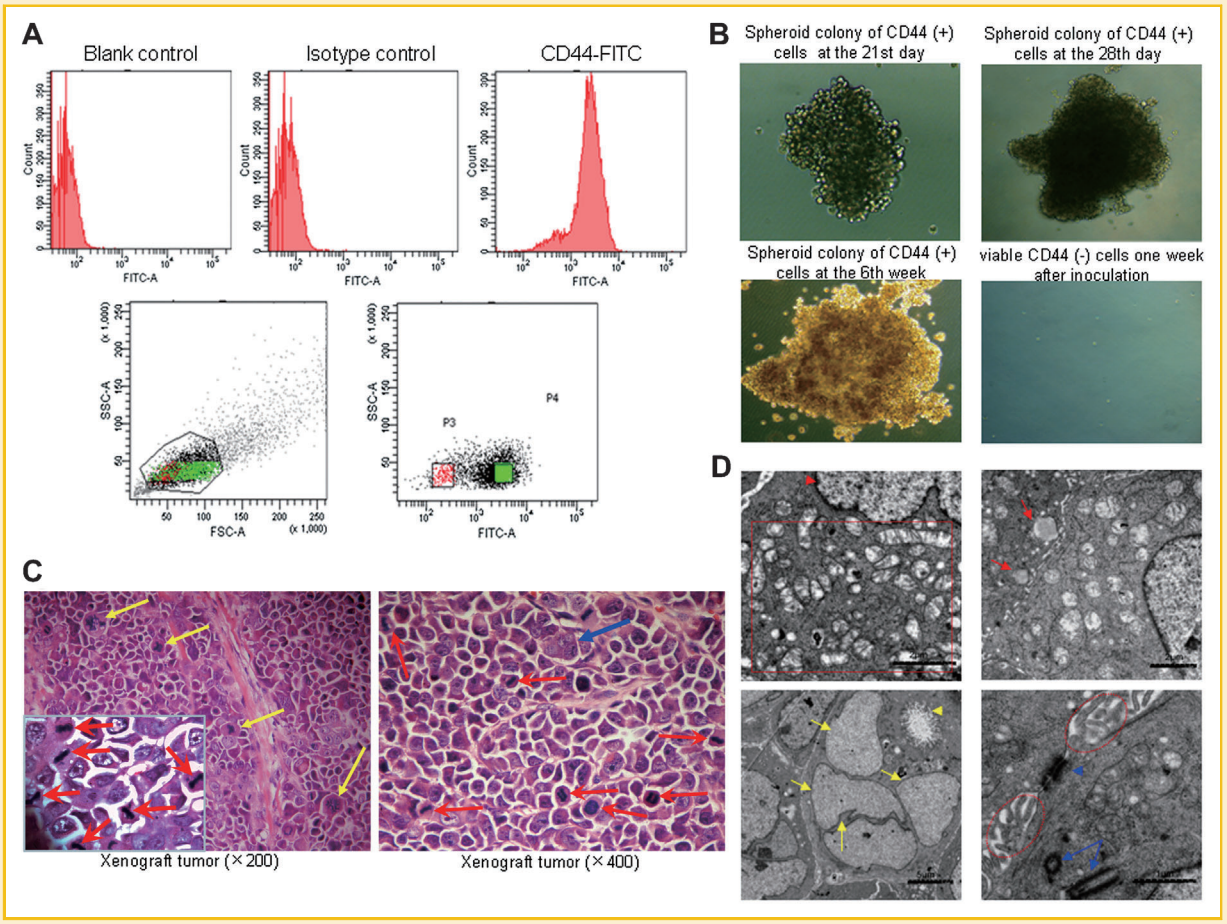

Fig. 2. Analysis of the cell surface marker CD44, SC formation, and the morphology of the xenograft tumors. A: CD44 expression. CD44 (+) and CD44 (−) cells were sorted using FACS. The CD44 (+) cells (green block) and the CD44 (−) cells (red spots) were collected separately. B: SC formation of the sorted cells (200×). The SC of the CD44 (+) cells remained on the 21st and 28th day and on the 6th week after inoculation. Several viable CD44 (−) cells remained 1 week after inoculation. C: HE staining of the tumor tissues from the tumor-bearing mice. Left: The cells grew in a disorderly fashion, and marked atypia and pathological karyokinesis were evident (yellow arrows) (200×). The magnified inset (1,000×) shows that the chromatin became condensed in many cells (red arrows), indicating that the cells were in mitosis. Right: A tumor giant cell with three nuclei (blue arrow) also exhibited atypia (400×). Many mitotic figures (10–45/1HPF) (red arrows in both images) indicated highly abnormal proliferation activity. All of the features were highly indicative of malignancy. D: Ultrastructure of the tumor tissues under TEM. The mitochondria proliferated ineffectually, resulting in a mass of hypoplastic mitochondria with underdeveloped double-membrane structures and partially fractured or swollen cristae (red dotted rectangle). Karyolobism and rich euchromatin were evident (red arrow head). Mucous granules (red arrows) are one of the features of gastrointestinal cancer. Polynucleation, accompanied by umbilication of karyotheca (yellow arrows), was observed; this process results in the enlargement of the karyotheca to satisfy the rapid metabolism. The intracellular microglandular cavity (yellow arrow head) is another feature of gastrointestinal cancer. Poorly developed desmosomes (blue arrow head) and flourishing microvilli on the surface of the cells (red ovals) were present. Abnormal enlarged centrosomes comprised of two mutually perpendicular centrioles were also observed (blue arrows).

repeated six times, the SC number averaged 670.3 ± 9.2; however, for the CD44 (−) fraction, which was conducted four times, only 1 SC formed. Thus, approximately 15% of the CD44 (+) cells were able to form SCs, whereas SC formation was rarely observed in the CD44 (−) cells.

SC-DERIVED CELLS GENERATED XENOGRAFT TUMORS IN VIVO

Based on the above procedure, we confirmed that not all of the CD44 (+) cells could form SCs. Furthermore, the SC-derived cells survived under serum-free and nonadherent culture conditions for a relatively long time, which is considered one of the phenotypes of CSCs [Liu et al., 2013]. Thus, we chose to conduct further experiments with the SC-derived cells. To compare the tumorigenicity of the SC-derived cells and the CD44 (−) cells, these cells were subcutaneously grafted into NOD/SCID mice. The SC-derived cells generated palpable tumors at the injection sites after 6–8 weeks, and 100% ($n = 6$) of the mice formed tumors. Nevertheless, injection of the CD44 (−) fraction did not produce a tumor, even when the observation period was extended to 12 weeks ($n = 6$).

We further observed the morphology of the tumors harvested from the mice. HE staining of the tumor tissues revealed high degrees of malignancy (Fig. 2C). The ultrastructure of the tumor tissues under TEM was consistent with that of gastrointestinal cancer and displayed flourishing microvilli on the surface of the cells (Fig. 2D, red ovals)

and polynucleation or karyolobism (Fig. 2D, red arrow head and yellow arrows, respectively). Additionally, in the cytoplasm, a mass of hypoplastic mitochondria (Fig. 2D, red dotted rectangle), mucous granules (Fig. 2D, red arrows), and an intracellular microglandular cavity (Fig. 2D, yellow arrow head) were observed. Furthermore, although desmosomes were the main cell–cell junctions, they were poorly developed (Fig. 2D, blue arrow head), and the volume of the centrosomes that comprised two mutually perpendicular centrioles was enlarged more than five times than that of normal centrosomes (Fig. 2D, blue arrows).

ACBP-3 PROLONGED THE TUMORIGENIC TIME OF THE SC-DERIVED CELLS IN VIVO

To determine whether ACBP-3 could affect tumorigenicity, healthy SC-derived cells, either from the ACBP-3 group or the control group, were inoculated into six NOD/SCID mice. The ACBP-3-treated cells were grafted into the left side of the axillary region in the mice, whereas the control cells were grafted into the right side of the axillary region of the same mice. Tumors at the right axillary were palpable after 9–11 days; however, on the left side, the tumors could be initially palpated after 26–28 days, suggesting that the tumorigenicity of the SC-derived cells treated with ACBP-3 was significantly postponed, averaging 27.2 days ($P < 0.01$). The tumor volumes were recorded from the 14th to 58th day after grafting. On the 58th day, two mice appeared moribund. The xenografts in the left armpit were much smaller than those in the right because of the shorter growing time ($P < 0.05$; Fig. 3A,B).

ACBP-3 AFFECTED THE RATIO AND CELL STATUS OF CD44 (+) CELLS AND CD44 (−) CELLS

MKN45 cells were treated with different doses of ACBP-3 for 48 h, and cells treated with NS served as a control. Flow cytometry analysis of the cells was performed three times. As shown in Figure 3C, in the control cells, the proportion of CD44 (+) cells averaged 90.7%; however, the proportion of CD44 (+) cells treated with 13 μg/ml ACBP-3 dropped to an average of 66.7%. Moreover, this proportion was decreased further to 62.5% and 53.1% after treatment with 19 and 25 μg/ml ACBP-3, respectively, indicating that ACBP-3 could dose-dependently inhibit the growth of the CD44 (+) cells ($P < 0.05$). As expected, the percentage of CD44 (−) was increased with increasing doses of ACBP-3 (13, 19, or 25 μg/ml), from 9.2% (control) to 31.5%, 35.6%, and 45.9%, respectively ($P < 0.05$; Fig. 3C, the upper panel; Supplementary Fig. S2A). We further investigated the cell status of the CD44 (−) cells and CD44 (+) cells. In the control group, 86.4% of the CD44 (−) cells and 97.3% of the CD44 (+) cells were healthy. However, in the 13 μg/ml ACBP-3 group, the CD44 (−) fraction was composed of 67.4% of healthy cells, 19.7% of apoptotic cells and 12.9% of dead cells, although the majority of the CD44 (+) cells remained healthy ($P < 0.05$). More cells died after treatment with increasing doses of ACBP-3: in the 19 μg/ml ACBP-3 group, the proportion of healthy CD44 (−) cells decreased to 48.9%; whereas, 88.4% of CD44 (+) cells were still healthy. Surprisingly, in the 25 μg/ml ACBP-3 group, the percentage of healthy CD44 (+) cells sharply declined to 32.5%; at the same time, the percentage of apoptotic cells increased to 66.3% in the CD44 (+) fraction. Moreover, the majority of the CD44 (−) cells were apoptotic and dead ($P < 0.05$; Fig. 3C, the middle and lower panel; Supplementary Fig. S2B,C).

ACBP-3 INHIBITED THE CLONE-FORMING CAPACITY OF THE SC-DERIVED CELLS

The effect of ACBP-3 on the clone-forming ability of the SC-derived cells was investigated. When treated with a continuous low dose of ACBP-3, no clone was able to form, although nearly 55% of the cells were alive, as confirmed by Trypan blue staining; however, the SC-derived cells that were not treated with ACBP-3 formed clones of different sizes, as displayed by Giemsa staining (Fig. 3D). The clone-forming efficiency of these cells averaged 87.4%.

ACBP-3 SUPPRESSED THE PROLIFERATION OF THE SC-DERIVED CELLS

To explore the effect of ACBP-3 on the growth of the SC-derived cells, the cells were treated with increasing doses of ACBP-3 for 24, 48, and 72 h. The survival rates were assessed using the MTS reagent, and the IR was calculated. The result showed that the IR at 24, 48, and 72 h was approximately zero in the vehicle control cells. However, as shown in Figure 4A, ACBP-3 treatment led to a dose-dependent inhibitory effect on cell growth. With exposure to 10, 13, 16, 19, 22, or 25 μg/ml ACBP-3 for 24 h, the survival rate of the SC-derived cells decreased by 5%, 8%, 15%, 18.5%, 19.8%, and 19.9%, respectively. This effect was persistent and prominent as the time of the treatment was prolonged; for example, treatment with 22 μg/ml ACBP-3 for 48 and 72 h inhibited the growth rate by 35.7% and 41.6%, respectively, compared with 19.8% at 24 h (Fig. 4A). We examined the morphology of the cells before and after ACBP-3 treatment. We found that before ACBP-3 treatment, approximately 50% of the SC-derived cells were living in suspension, whereas the other 50% of the cells were anchorage-dependent (Fig. 4B). However, after treatment with ACBP-3 (22 μg/ml) for 48 h, most of the SC-derived cells were in suspension. Additionally, cell membrane integrity was lost, and the leakage of cytoplasmic materials occurred (Fig. 4B, red arrow).

The ultrastructure of the cells was further investigated. Before ACBP-3 treatment, exuberant microvilli and pseudopodia with fourth or fifth branches were evident on the surface of the SC-derived cells. Cell divisions were evident, and the cell shapes and sizes varied (Fig. 4D, control). Hypertrophied nuclei (Fig. 4C, red arrow), multi-nucleoli (Fig. 4C, blue arrows), loose intercellular junctions (Fig. 4C, blue arrow head), and overly developed microfilaments (Fig. 4C, red arrow head) were observed in these cells. Comparatively, when exposed to 16 μg/ml ACBP-3 for 48 h, the numbers of microvilli and pseudopodia were remarkably reduced, and many vesicular protuberances appeared on the cell membranes (Fig. 4D, 16 μg/ml ACBP-3). The microvilli disappeared and almost all of the pseudopodia had obvious holes (Fig. 4D, red arrow head) or were even dissolved (Fig. 4D, red arrow) in the case of treatment with 22 μg/ml ACBP-3 (Fig. 4D, 22 μg/ml ACBP-3). The intracellular ultrastructure showed apoptotic characteristics (Fig. 4C, black arrow, black arrow head, and red rectangle). Figure 4E further demonstrated that treating cells with 22 μg/ml ACBP-3 significantly promoted cell apoptosis (apoptotic rate 67.89% ± 6.43 in ACBP-3 cells, whereas, only 5.76% ± 2.39 in control cells, $P < 0.01$).

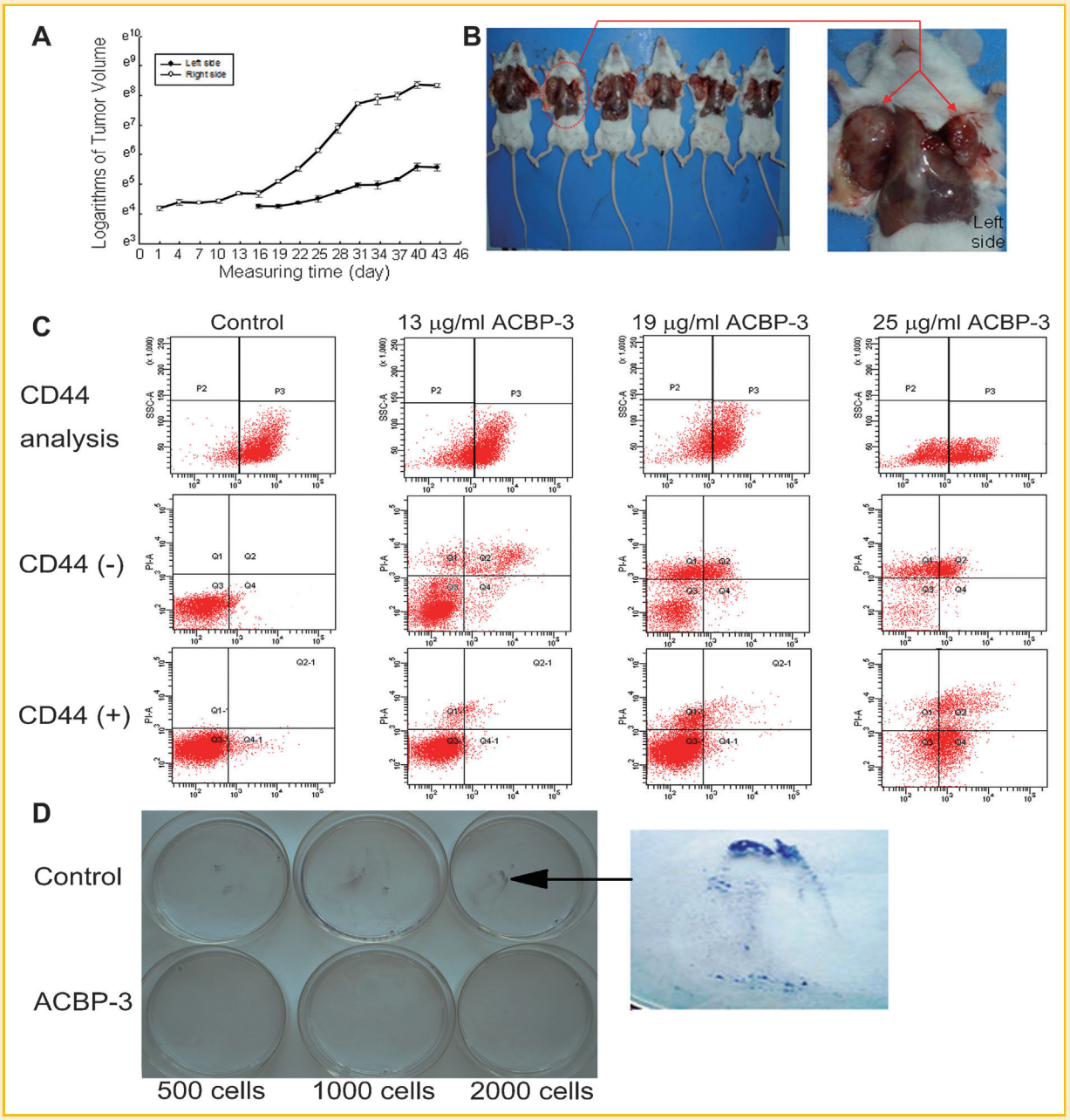

Fig. 3. Effects of ACBP-3 on the tumorigenicity and colony-forming capacity of the MKN45 SC-derived cells, and on the percentage of CD44 (+) and CD44 (−) fraction. A: The natural logarithm curves of the xenograft tumor volume in both axillary regions of the NOD/SCID mice. B: Left: NOD/SCID mice with xenograft tumors. Right: magnified image of the indicated mouse. C: Flow cytometry analysis to determine the proportion of CD44 (+) and CD44 (−) cells in the MKN45 cell line treated with different doses of ACBP-3. Upper panel: The percentage variation of the CD44 (+) cells and CD44 (−) cells in MKN45 cells treated with different doses of ACBP-3. Middle and lower panels: The cell status of the CD44 (−) fraction and the CD44 (+) fraction, respectively. D: Decline in the clone forming ability of the cells treated with a continuous low dose of ACBP-3. The culture dishes were inoculated with 500, 1,000, and 2,000 SC cells. The cells that were not treated with ACBP-3 formed colonies, as shown by Giemsa staining; the cells treated with ACBP-3 treatment formed no colonies. Right image: Magnification of the indicated cell colony.

ACBP-3 ACCELERATED THE APOPTOSIS OF THE SC-DERIVED CELLS TIME-DEPENDENTLY

To verify the apoptotic effect of ACBP-3 on the SC-derived cells, the expression of caspase-3, Bax and Bcl-2 were measured. As shown in Figure 4F, treating cells with 22 μg/ml ACBP-3 increased the expression of caspase-3 and Bax, while it decreased the expression of Bcl-2 at 24 h. When the treatment time was prolonged, the expression of caspase-3 and Bax was further enhanced, while Bcl-2 expression gradually decreased ($P < 0.05$).

ACBP-3 DECREASED THE EXPRESSION OF F-ACTIN IN THE MKN45 SC-DERIVED CELLS

It is well known that F-actin is highly expressed in microvilli and pseudopodia. Because the numbers of microvilli and pseudopodia

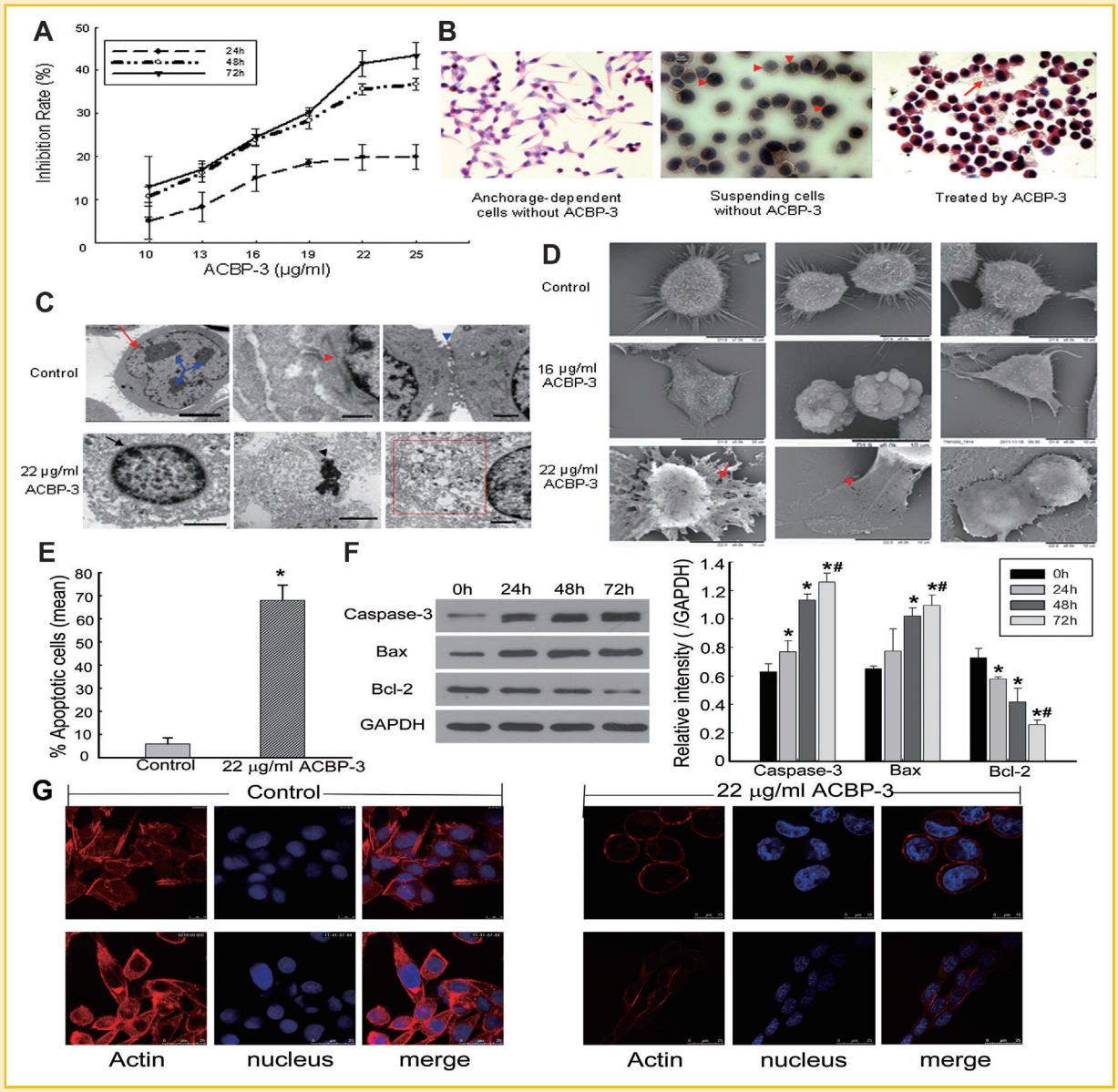

Fig. 4. Inhibitory effect of ACBP-3 on the MKN45 SC-derived cells. A: ACBP-3 suppressed the proliferation of the SC-derived cells in a time- and dose-dependent manner. B: Morphology of the SC-derived cells under a light microscope. The suspension cells were spherical in appearance with hypertrophied nuclei (red arrow heads) that occupied more than 90% of the cytoplasm in some cells. The anchorage-dependent cells were spindle- and fusiform-shaped. The red arrow indicates leaked cytoplasm. C: Ultrastructural changes in the SC-derived cells treated with ACBP-3, as observed by TEM. Red arrow: hypertrophied nuclei; blue arrows: multi-nucleoli; red arrowhead: overly developed microfilaments; blue arrowhead: loose intercellular junction; black arrow: condensed chromatin under the nuclear envelope; black arrow head: appearance of pyknotic nucleus during the late stage of apoptosis; red rectangle: vacuolar degeneration in the cytoplasm. D: Ultrastructure of the SC-derived cells before and after ACBP-3 treatment, as observed by SEM. The red arrow and arrowhead indicate the dissolved and punched pseudopodia of the cells, respectively, when treated with 22 μg/ml ACBP-3 for 48 h. E: Quantification of the apoptotic cells observed by electron microscopy. $^{*}P < 0.01$ compared to the control. F: The expression of caspase-3, Bax, and Bcl-2 were verified by Western blot analysis and evaluated by the graphic quantification of the band density. $^{*}P < 0.05$ compared to the control; $^{\#}P < 0.05$ compared to the 24 h group. G: Confocal analysis of F-actin.

were reduced in the ACBP-3-treated cells (Fig. 4D), we want to confirm that F-actin expression was simultaneously decreased. Figure 4G shows that F-actin was located in the cell membrane and the cytoplasm in the control cells. Flourishing microvillus-like or pseudopodium-like structures were observed on the cell surface (Fig. 4G, Control). Compared to the control, the fluorescence intensity of F-actin in the ACBP-3-treated cells was obviously weakened. F-actin expression on the membrane and in the cytoplasm was obviously reduced. Interestingly, the microvillus-like or pseudopodium-like structures disappeared, consistent with the ultrastructural changes that were observed (Fig. 4G, 22 μg/ml ACBP-3).

ACBP-3 SUPPRESSED XENOGRAFT TUMOR GROWTH IN VIVO

The biological activity of ACBP-3 was examined after modeling and grouping NOD/SCID mice. The grouped tumor-bearing mice were treated with ACBP-3, cisplatin, or a combination of ACBP-3 and

cisplatin. NS was injected as a control (detailed in Materials and Methods Section). Data were recorded for more than 4 weeks until the cisplatin-treated mice appeared to display symptoms of a severe toxic reaction and impending death. ACBP-3, cisplatin, and the combination treatments all suppressed tumor growth compared to the control ($P < 0.05$; Fig. 5A,B). The tumor inhibition rates were 43.32%, 66.94%, and 73.68% for ACBP-3, cisplatin, and the combination treatment, respectively (Fig. 5C). When treatment was prolonged, the tumor-suppressing effect of the combination treatment, followed by cisplatin, were more efficient than that of ACBP-3 alone ($P < 0.05$); however, there was no significant difference between the cisplatin treatment alone and its combination with ACBP-3 (Fig. 5B,D,E).

ACBP-3 WAS LESS TOXIC TO THE MICE

Although the present results indicated that ACBP-3 is an efficient antitumor agent, we were interested in whether ACBP-3 is less toxic than cisplatin. As shown in Figure 6A, application of cisplatin alone or its combination with ACBP-3 caused significant losses in the body weight of the mice. However, in the later period of the treatment, the weights of the cisplatin-treated mice were lower than those of the combined-treated group ($P < 0.05$). The lowest body weight in the cisplatin-treated mice dropped to 12.2 g, leading to the impending death of the mouse; this suggests that the combination of cisplatin and ACBP-3 could partially alleviate the body weight loss in the mice. Compared with the body weights of the mice treated with cisplatin alone or with the combination treatment, ACBP-3 administration did not significantly affect the body weight of the mice ($P < 0.05$). Moreover, in the healthy animals, no difference was observed in the appearance, body weight, feeding or living status between the ACBP-3-administered mice and the controls ($P > 0.05$).

ACBP-3 INDUCED TUMOR NECROSIS

The microstructure and ultrastructure alterations of the tumor tissues were examined. Compared to the control, localized necrosis could be

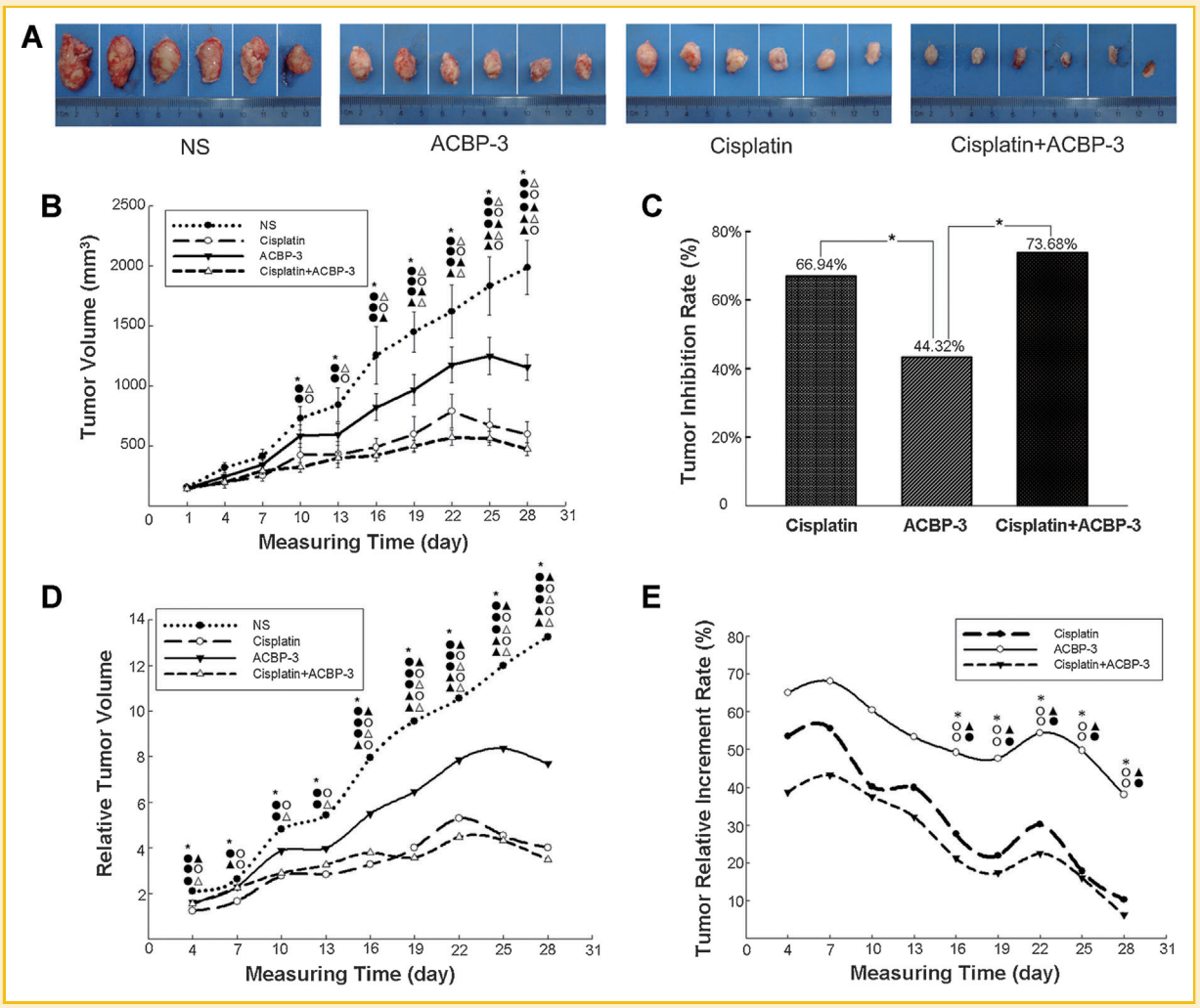

Fig. 5. ACBP-3 suppressed xenograft tumor growth. A: Tumors from the xenograft model mice. The mice in the four groups were administered different reagents (n = 6) before they were sacrificed. B: Tumor growth curve. The tumor volumes were expressed as the mean ± standard errors. $^{*}P < 0.05$. C: The tumor inhibition rate of the xenografts in mice treated with ACBP-3, cisplatin, and ACBP-3 plus cisplatin. $^{*}P < 0.05$. D: The curve of the relative tumor volume. $^{*}P < 0.05$. E: The curve of the tumor relative increment rate, $^{*}P < 0.05$.

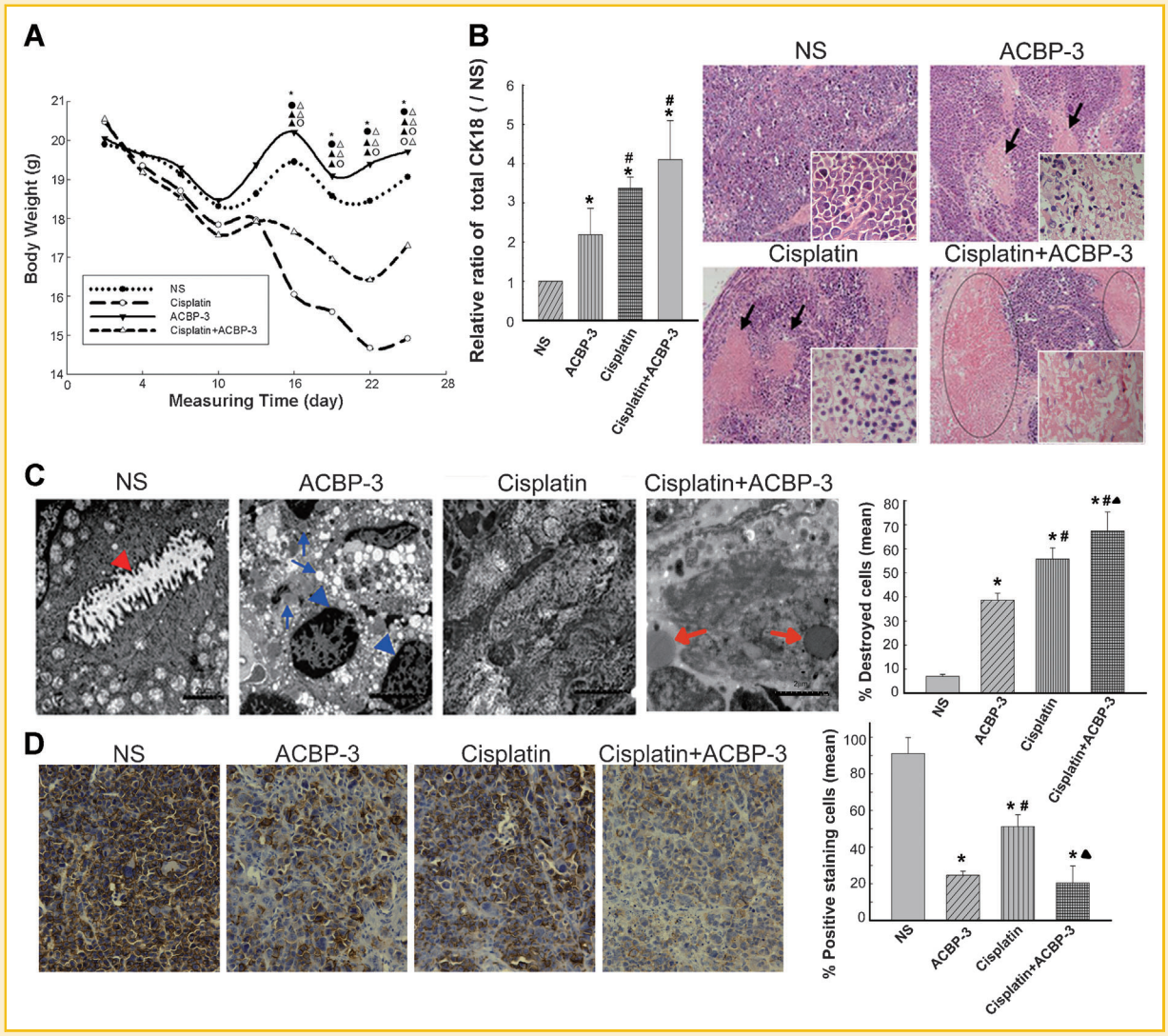

Fig. 6. Effects of ACBP-3 on the body weight of the mice and the morphological features of tumors in each group. A: The body weight of each group. The body weight was checked at every time point. $^{*}P < 0.05$. B: Relative ratio of total CK18 and HE staining of the tumors from each groups. Right panel: Localized necrosis and large patches of necrosis are indicated by the arrows and oval circles, respectively. The micrographs were acquired under a light microscope with 100× magnification. The image in the right lower corner of each micrograph was magnified 400×. Left: The ratios of the relative CK18 levels in the drug treatment groups were compared to the NS treatment; $^{*}P < 0.05$ compared to the NS group; $^{\#}P < 0.05$ compared to the ACBP-3 group. C: The ultrastructure of the tissues from the four groups. The glandular cavity with microvilli on the interior surface is indicated by the red arrowhead; mucoproteins and slime substances were observed in this cavity. Lipid droplets and vacuoles appeared in the cytoplasm (blue arrows); nuclear chromatin condensed into several large homogeneous masses and was observed close to the nuclear envelope (blue arrowheads). Lipid vacuoles are indicated by red arrows. Histogram: Graphic quantification of the destroyed cells in the tumor tissues of the different groups. $^{*}P < 0.05$ compared to the NS group; $^{\#}P < 0.05$ compared to the ACBP-3 group; $^{\blacktriangle}P < 0.05$ compared to the cisplatin group. D: Immunohistochemistry analysis of CD44 expression. Histogram: Graphic quantification of positively stained cells. $^{*}P < 0.05$ compared to the NS group; $^{\#}P < 0.05$ compared to the ACBP-3 group; $^{\blacktriangle}P < 0.05$ compared to the cisplatin group.

observed everywhere in the ACBP-3 and cisplatin groups (Fig. 6B, arrows), whereas large patches of necrosis were observed in the combined medication group (Fig. 6B, shown by oval circles).

To biochemically evaluate the extent of the tumor tissue necrosis, total plasma CK18 was detected in the mice. The relative ratio of total CK18 [(A/V)/(B/VN)] was calculated (for explanation of this formula, please refer to the Materials and Methods Section). Compared to the NS group (its relative ratio = 1), the relative ratios of CK18 in the mice before drug treatment were 0.938 ± 0.097, 1.052 ± 0.104, and 0.993 ± 0.221 for the ACBP-3, cisplatin, and combination groups, respectively. The values among the three groups before drug treatment were not significantly different from those in the NS group. However, after drug treatment, the relative ratios of CK18 in the three groups were 2.187 ± 0.675, 3.367 ± 0.289, and 4.129 ± 0.984 ($P < 0.05$) for the ACBP-3, cisplatin, and combination groups, respectively, compared to the NS group. The remarkable elevation in the relative ratio of the biochemical indicator CK18 suggested the tumor tissue necrosis was more severe in the mice after receiving the drug treatment. Additionally, the ratios of the ACBP-3 group and the cisplatin group were significantly different ($P < 0.05$),

as were those of the ACBP-3 group and the combination group. No significant differences were observed between the cisplatin group and the group treated with both cisplatin and ACBP-3 (Fig. 6B, histogram).

Ultrastructural examination revealed several interesting changes. In the NS group, a glandular cavity with microvilli on the interior surface and mucoproteins and slimy substances in the cavity was observed (Fig. 6C, red arrow head). In the ACBP-3-treated group, the appearance of a large amount of lipid droplets and vacuoles (Fig. 6C, blue arrows) was observed in the cytoplasm, as well as the presence of typical apoptotic nuclei with chromatin condensed into several large homogeneous masses close to the nuclear envelope (Fig. 6C, blue arrow heads). In the cisplatin-treated group, disrupted and fused cell structures were observed. In the combined medication group, severely destroyed tumor tissue structures were observed, as well as cytolysis and lipid vacuoles (Fig. 6C, red arrows). These results implied that the antitumor effects of ACBP-3 and cisplatin might be synergistically strengthened if they are combined. Graphic quantification revealed that destroyed cells comprised 38.68%, 56.73%, and 67.46% of the tissue in the ACBP-3, cisplatin and combination groups, respectively ($P < 0.05$) (Fig. 6C).

ACBP-3 DECREASED THE PROPORTION OF THE CD44 (+) FRACTION IN THE TUMOR TISSUE

The proportion of CD44 (+) cells in MKN45 cell culture was reduced by ACBP-3 treatment, as described above. Therefore, the proportion change of the CD44 (+) in the tissue slides was further examined using immunohistochemistry. The results showed that the CD44 (+) cells in all three drug-treated groups significantly decreased compared to the NS group ($P < 0.05$). The CD44 (+) cells in the ACBP-3 group and in the combination group were lower than those in the cisplatin group ($P < 0.05$), suggesting that the ability of ACBP-3 to reduce the number of CD44 (+) cells in the tumor tissue was superior to that of cisplatin. When combined with ACBP-3, this ability was strengthened in spite of the decreased dose (Fig. 6D).

ACBP-3 SUPPRESSED THE SC-DERIVED CELLS IN ANOTHER HUMAN GASTRIC CELL LINE

To investigate the relevance of the previous results, another human gastric cell line, MKN74, was used to determine whether the results shown above were cell line specific. First, the MKN74 cells with CSC characteristics were identified. The CD44 (+) cells were sorted using FACS, and the percentage of these cells averaged 85.1% (Fig. 7A). Additionally, some of the CD44 (+) cells formed SCs, and the SC-forming cell population contained approximately 22% of the CD44 (+) MKN74 cells (Fig. 7B, upper image). The tumorigenicity of the CD44 (+) SC-derived cells were tested, and all of the grafted NOD/SCID mice generated xenograft tumors ($n = 4$) (Fig. 7B, bottom image). In contrast, the CD44 (−) cells were unable to produce xenograft tumors.

The effect of ACBP-3 on the clone-forming ability of the SC-derived cells was then tested. The clone-forming efficiency averaged 96.7% in the control group, but it dropped to an average of 34.7% when cells were treated with ACBP-3 (Fig. 7C).

We examined whether ACBP-3 could decrease the proportion of CD44 (+) cells in the MKN74 cell line as it did in the MKN45 cell line. Flow cytometry was used to answer this question. MKN74 cells were treated with different doses of ACBP-3 for 48 h, and NS-treated cells served as a control. The percentage of CD44 (+) cells declined to 53.4% and 32.6% when the MKN74 cells were treated with 13 and 19 μg/ml ACBP-3, respectively ($P < 0.05$); on the other hand, the CD44 (+) cells comprised approximately 85.9% of the MKN74 cells in the control group ($P < 0.05$). The percentage of CD44 (−) increased to 45.8 and 65.6% when the cells were treated with 13 and 19 μg/ml ACBP-3, respectively ($P < 0.05$); these changes were significantly different than the 12% observed in the control group ($P < 0.05$; Fig. 7D, upper panel; Supplementary Fig. S2D). The percentages of apoptotic, dead, and healthy cells within the CD44 (−) cells and CD44 (+) populations were further examined at different doses of ACBP-3. Prior to treatment, the majority of the CD44 (−) cells (99%) and 94.3% of the CD44 (+) cells were healthy. However, after treatment with 13 μg/ml ACBP-3, the CD44 (−) cells were composed of 68.9% healthy cells, 10.9% apoptotic cells, and 20.1% dead cells ($P < 0.05$). Moreover, only 1.7% of the CD44 (−) cells remained healthy, and the majority of the CD44 (−) cells were apoptotic (96.8%) in the 19 μg/ml ACBP-3 group ($P < 0.05$) (Fig. 7D, middle panel; Supplementary Fig. S2E). Furthermore, the percentage of the healthy cells in the CD44 (+) fraction declined to 57.9% and 12.6%, the percentage of apoptotic cells soared to 26% and 87.2%, and the percentage of dead cells were 19% and 5.4% in the 13 and 19 μg/ml ACBP-3 groups, respectively ($P < 0.05$; Fig. 7D, bottom panel; Supplementary Fig. S2F).

The ability of ACBP-3 to suppress the proliferation of the SC-derived cells was investigated using the MTS reagent. As shown in Figure 7E, similar to the effect observed in the SC-derived cells of the MKN45 cell line, the growth of the SC-derived cells of the MKN74 cell line was also inhibited in dose- and time-dependent manners, and growth was inhibited by up to 70%, whereas the rate at the corresponding time and dose in the MKN45 cell line was 41.6%. The morphological features of the SC-derived cells before and after ACBP-3 treatment were also observed, and the changes were apparent (Fig. 7E).

Additionally, the expression levels of apoptosis-related proteins were examined in the MKN74 cell line, and the pro-apoptotic effect of ACBP-3 was confirmed (Fig. 7F).

We applied the same procedures as the MKN45 cell line to verify the prolonged effect of ACBP-3 on the tumor formation time of the MKN74 SC-derived cells in vivo, and similar results were obtained (Fig. 7G).

DISCUSSION

For the first time, we preliminarily analyzed the components of ACBP-3. The main component of ACBP-3 is an ubiquitin-like substance. The other major component is a fatty acid-binding protein (FABP). Thus far, many anticancer therapeutic interventions have been developed to target certain steps in the ubiquitination pathway [Burger and Seth, 2004; Petroski, 2008; Chitra et al., 2012]. The ubiquitin-like substance identified in the ACBP-3 components may perform an anticancer function by identifying certain oncogenic proteins, tagging them and directing them to the ubiquitin-proteasome system (UPS), thereby leading to their degradation. Alternatively, the ubiquitin-like substance in ACBP-3 might

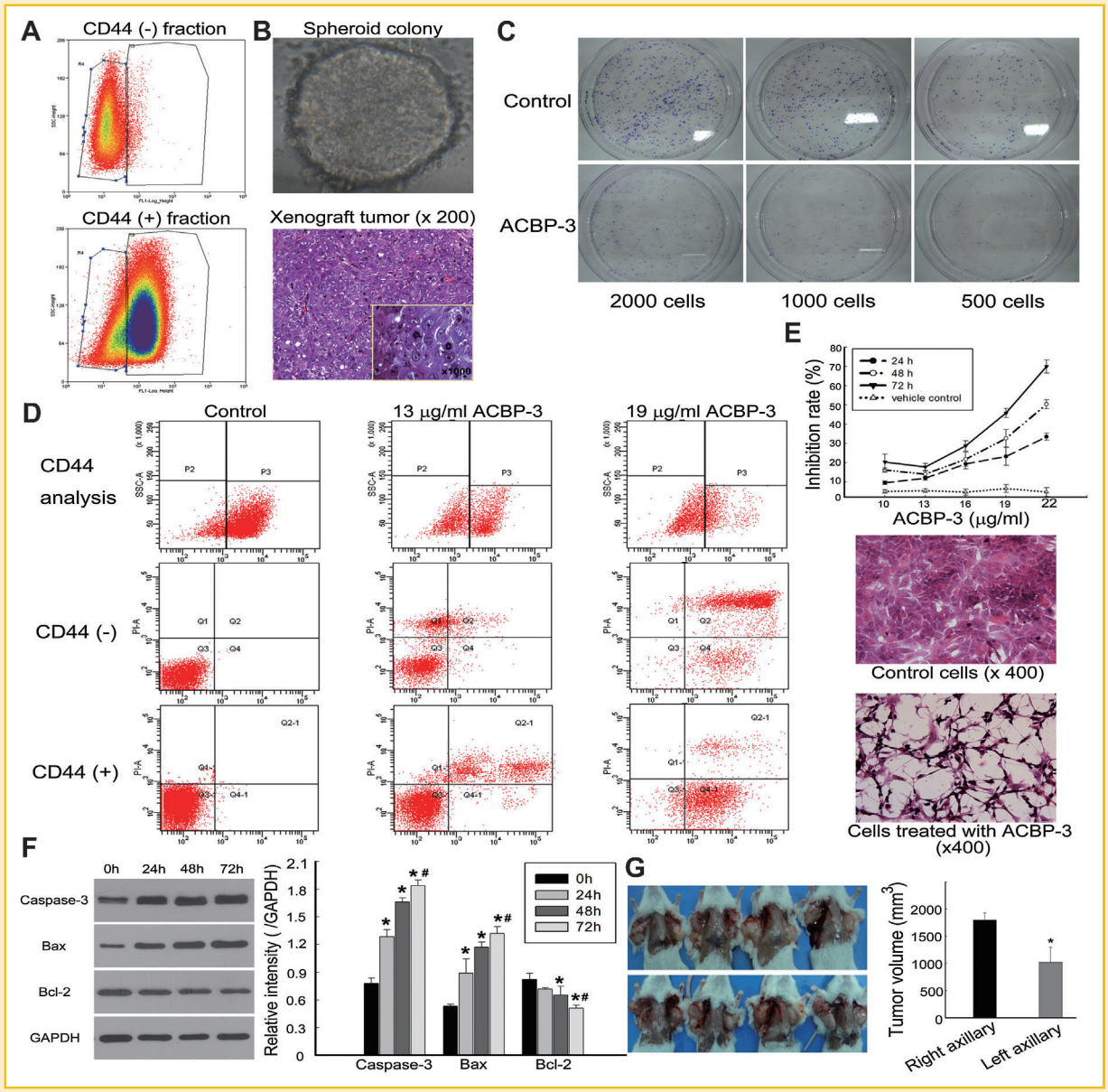

Fig. 7. Effect of ACBP-3 on the MKN74 human gastric cancer cell line. A: Flow cytometric analysis and FACS of CD44 expression. Upper image: The CD44 (−) MKN74 cells were sorted. Bottom image: The CD44 (+) MKN74 cells were sorted. B: CSC nature of the CD44 (+) MKN74 cells. Top panel: A SC formed by the CD44 (+) cells. Bottom: HE staining of xenograft tumors generated from the SC-derived cells. The inset to the lower right is a partial magnification (1,000×). C: The effect of ACBP-3 on the clone-forming ability of the SC-derived cells. D: Flow cytometric analysis of the proportions of the CD44 (+) and CD44 (−) fractions in MKN74 cells treated with different doses of ACBP-3. Top panel: The percentage variation of CD44 expression in MKN74 cells treated with different doses of ACBP-3. Middle and lower panels: The cell status in the CD44 (−) and CD44 (+) fraction, respectively. E: Inhibitory effects of ACBP-3 on the SC-derived cells. Top: ACBP-3 suppressed the proliferation of the SC-derived cells in a time- and dose-dependent manner. *X*-axis: different doses of ACBP-3; *Y*-axis: inhibition rate of the SC-derived cells by ACBP-3. Middle panel: The SC-derived cells from the MKN74 cell line prior to ACBP-3 treatment. The cells compactly grew with ample cytoplasm. Bottom panel: The SC-derived cells of the MKN74 cell line treated with ACBP-3. The cytoplasm was significantly reduced, resulting in a dry branch-like appearance. F: Left: The expression of caspase-3, Bax, and Bcl-2 were verified by Western blot analysis. Right: Graphic quantification of the relative band density. $^{*}P < 0.05$ compared to the control; $^{\#}P < 0.05$ compared to the 24 h group. G: NOD/SCID mice with xenograft tumors. Left: Image of the tumor-bearing mice. The same numbers of healthy SC-derived cells that were both Annexin V negative and PI negative were subcutaneously grafted into the axillary region. The ACBP-3 treated cells were inoculated in the left axillary regions of 8-week-old NOD/SCID mice, while the control cells were inoculated into the right axillary regions. Right: Histogram of the tumor volume in both axillary regions. $^{*}P < 0.05$ compared to the control.

competitively bind to tumor suppressor proteins but not play an ubiquitin-tagging role, thereby protecting the tumor suppressor protein from degradation by the UPS. Some FABPs are thought to transport lipophilic molecules from the outer cell membrane to certain intracellular receptors, such as PPAR, in order to perform certain biological functions [Tan et al., 2002; Chmurzynska, 2006]. Moreover, PPAR-α has been reported to possess anticancer properties by affecting the energy balance of the cancer cells, forcing glycolysis-

dependent cancer cells to die as a result of metabolic catastrophe [Grabacka and Reiss, 2008]. Presumably, FABP, as an ACBP-3 component, might transport certain molecules to PPAR-α, promoting the anticancer activity of PPAR-α. Further identification of the components of ACBP-3 and their respective anticancer mechanisms should be the focus of future research.

Cisplatin, as one of the most widely used antineoplastic medications, is often used together with other anti-cancer drugs. However, the toxicity of cisplatin is its Achilles′ heel [Chu et al., 2010]. Increasing toxicity has been found when cisplatin is combined with other classic chemotherapeutic medications [Ajani, 2008]. Thus, researchers have been focusing on developing potential bioactive substances that have both minimal toxicity and maximal tumor-suppressing efficacy. The peptide used in this study, ACBP-3, provides a new prospect that may have potential for clinical applications.

To elucidate the mechanism of action of ACBP-3, we focused on its anti-cancer effects in GCSCs. Evidence for GCSCs was seldom reported until Takaishi et al. analyzed six human gastric cancer cell lines with defined surface markers that had been verified as CSC markers in other cancers. Their results firmly showed that GCSCs existed in the CD44 (+) fraction [Takaishi et al., 2009]. Additionally, Takaishi et al. [2009] showed that among the cell lines they studied, the MKN45 cell line possessed the highest percentage of CD44 (+) cells, and the MKN74 cell line had the second highest percentage. Their findings, together with other studies, confirmed that the side population cells were not enriched with GCSCs [Burkert et al., 2008; Takaishi et al., 2009; She et al., 2012]. Accordingly, the human gastric cancer cell line MKN45, followed by the MKN74 cell line, was the preferred cell line to study these cells. Sorting the CD44 (+) cells was the first hurdle for identifying the CSCs in our research.

Currently, two main experimental procedures have been widely adopted to identify candidate cells as CSCs: SC formation capacity under specific culture conditions and xenograft tumor-generating ability in immunodeficient mice [Clarke et al., 2006].

In our study, we first observed the SC-forming capacity of the CD44 (+) fraction of the MKN45 human gastric cancer cell line in vitro. We verified that approximately 15% of the CD44 (+) cells were able to form SCs, which is consistent with the results reported by Takaishi et al. [2009]. The tumorigenicity of the SC-derived cells also verified their CSC nature. Therefore, the SC-derived cells were regarded as GCSCs in our study.

In an in vitro study, we found that ACBP-3 suppressed the proliferation of the SC-derived cells in a time- and dose-dependent manner (Fig. 4A,E). Morphological examination showed that the cells exhibited apoptotic features. The detection of apoptosis-related proteins also confirmed the pro-apoptosis efficacy of ACBP-3. Flow cytometry results showed that increasing doses of ACBP-3 led to a decrease in the percentage of CD44 (+) cells, while the percentage of CD44 (−) cells increased accordingly; both apoptotic and dead cells increased in the CD44 (−) fraction. Although unhealthy cells in the CD44 (+) cells increased slightly when the dose of ACBP-3 was low (13 μg/ml), such a tendency was dramatically changed when cells were treated with 19 μg/ml ACBP-3, resulting in the accumulation of dead or apoptotic cells (Figs. 3C and 7D). The results indicated that ACBP-3 could induce the CD44 (+) cells to convert to CD44 (−) cells, as well as induce cell death and apoptosis. In vivo, we confirmed that the SC-derived cells treated with ACBP-3 took significantly longer to form tumors compared to the control treated cells (Fig. 3A,B). For this experiment, we inoculated the mice with the healthy SC-derived cells sorted by FACS to avoid the cells that had already initiated apoptosis. The results showed that ACBP-3 could affect the tumorigenesis of the SC-derived cells. Given the above results, it was possible that ACBP-3 could induce the differentiation of the SC-derived cells into CD44 (−) cells, which were more differentiated and easily destroyed by the medications. When mice bearing xenograft tumors were treated with the drugs, the tumor inhibition rate of ACBP-3 was 43.32%. Combined treatment with ACBP-3 and cisplatin resulted in the most powerful tumor-suppressing potency, with an inhibition rate of 73.68%; however, the dose of each agent in the combined treatment was half of that used as a single agent.

We further detected the total CK18 levels to measure the extent of tumor tissue necrosis across the four groups. Circulating intact and caspase-cleaved forms of CK18 are regarded as biomarkers of the chemotherapy-induced cell death of tumors [de Haas et al., 2008]. Apoptosis and necrosis result in the release of caspase-cleaved CK18 fragments and intact CK18, respectively [Olofsson et al., 2007; Oyama et al., 2012]. The M65 ELISA assay measures the levels of total CK18, including both the caspase-cleaved and intact CK18 forms [Scott et al., 2009]. Moreover, the M65 assay does not detect mouse CK18; therefore, the biomarker data obtained from the tumor-bearing mice were derived from the human xenograft tumor. Thus, the total CK18 measured by this method is a reliable measure of the events occurring within the tumor [Micha et al., 2008]. In our study, no significant difference was observed at the baseline of the four groups, according to the M65 ELISA, excluding the effects due to natural biological variation; therefore, the data closely reflected the drug-induced tumor-specific changes in CK18. Other research has also shown that any elevations of CK18 in the plasma of xenograft-bearing animals are almost exclusively derived from the tumor [Cummings et al., 2008]. Throughout the course of xenograft tumor growth and medication-induced cell death in tumors, researchers found a positive correlation between the level of circulating total CK18 and the tumor volume [Micha et al., 2008]. In light of this, we recorded the data as the ratio of the ELISA reading to the corresponding tumor volume. The results showed that the cell death of each drug-treatment group was more severe than that of the NS-treatment group ($P < 0.05$). The extent of necrosis in the combined group was the most severe, which is consistent with the results of the TEM observation. Although the necrosis in the cisplatin group was similar to that in the combined group, a dramatic drop in body weight and impending death was exhibited in the cisplatin group, resulting in the cessation of the medication. However, the survival status of the mice treated with the combination therapy was reassuring because the dose of cisplatin in the combination treatment was half of that used in the cisplatin group, and the presence of ACBP-3 in the combination treatment diminished the effect cisplatin had of the mouse′s body weight. Immunohistochemistry analysis of CD44 in the tumor revealed that ACBP-3 could decrease the amount of CD44 (+) cells in the tumor more effectively than cisplatin; when ACBP-3 and cisplatin were combined at half dose, the CD44 (+) cells in the tumor were more effectively eliminated (Fig. 6D). Additionally, most of the experiments were repeated in another human gastric cancer cell line,

MKN74, and the results of these experiments suggested that the inhibitory effect of ACBP-3 on GCSCs were not cell line specific.

To identify the mechanism of the anti-GCSC effect of ACBP-3, microRNA arrays are being used to detect the differences in the expression profile of microRNAs between the ACBP-3 treated and the untreated SC-derived cells. The changes in the CSC-specific microRNAs will be the focus of that study. The target genes and pathways will be predicted, and the tissue microarrays will be conducted. The results will be reported in the near future.

Together, our results clearly confirmed that the SC-derived cells possess the characteristics of CSCs. ACBP-3 suppressed GCSCs either in vitro or in vivo, suggesting that ACBP-3 could be a potential CSC-targeted agent. Importantly, ACBP-3 enhanced the chemotherapy tolerance of mice by reducing the toxicity of the treatment, as well as the effective dose of cisplatin. Our results demonstrated that the combination of cisplatin and ACBP-3 might be an effective way to clinically treat patients with cancer with a lower dose and reduced toxicity.

ACKNOWLEDGEMENTS

Most of the experimental work was completed in the Municipal Key Laboratory for Liver Protection and Regulation of Regeneration, Beijing, China.

REFERENCES

Ajani JA. 2008. Optimizing docetaxel chemotherapy in patients with cancer of the gastric and gastroesophageal junction: evolution of the docetaxel, cisplatin, and 5-fluorouracil regimen. Cancer 113:945–955.

Burger AM, Seth AK. 2004. The ubiquitin-mediated protein degradation pathway in cancer: Therapeutic implications. Eur J Cancer 40:2217–2229.

Burkert J, Otto WR, Wright NA. 2008. Side populations of gastrointestinal cancers are not enriched in stem cells. J Pathol 214:564–573.

Chitra S, Nalini G, Rajasekhar G. 2012. The ubiquitin proteasome system and efficacy of proteasome inhibitors in diseases. Int J Rheum Dis 15:249–260.

Chmurzynska A. 2006. The multigene family of fatty acid-binding proteins (FABPs): function, structure and polymorphism. J Appl Genet 47:39–48.

Chu KM, Ngan MP, Wai MK, Yeung CK, Andrews PL, Percie du Sert N, Lin G, Rudd JA. 2010. Olvanil, a non-pungent vanilloid enhances the gastrointestinal toxicity of cisplatin in the ferret. Toxicol Lett 192:402–407.

Clarke MF, Dick JE, Dirks PB, Eaves CJ, Jamieson CH, Jones DL, Visvader J, Weissman IL, Wahl GM. 2006. Cancer stem cells—Perspectives on current status and future directions: AACR Workshop on cancer stem cells. Cancer Res 66:9339–9344.

Cummings J, Hodgkinson C, Odedra R, Sini P, Heaton SP, Mundt KE, Ward TH, Wilkinson RW, Growcott J, Hughes A, Dive C. 2008. Preclinical evaluation of M30 and M65 ELISAs as biomarkers of drug induced tumor cell death and antitumor activity. Mol Cancer Ther 7:455–463.

de Haas EC, di Pietro A, Simpson KL, Meijer C, Suurmeijer AJ, Lancashire LJ, Cummings J, de Jong S, de Vries EG, Dive C, Gietema JA. 2008. Clinical evaluation of M30 and M65 ELISA cell death assays as circulating biomarkers in a drug-sensitive tumor, testicular cancer. Neoplasia 10:1041–1048.

Dickson MA, Carvajal RD, Merrill AH, Jr., Gonen M, Cane LM, Schwartz GK. 2011. A phase I clinical trial of safingol in combination with cisplatin in advanced solid tumors. Clin Cancer Res 17:2484–2492.

El-Bialy NS, Rageh MM. 2013. Extremely low-frequency magnetic field enhances the therapeutic efficacy of low-dose cisplatin in the treatment of Ehrlich carcinoma. Biomed Res Int 2013:189352.

Grabacka M, Reiss K. 2008. Anticancer properties of PPARalpha-effects on cellular metabolism and inflammation. PPAR Res 2008:930705.

Jemal A, Bray F, Center MM, Ferlay J, Ward E, Forman D. 2011. Global cancer statistics. CA Cancer J Clin 61:69–90.

Kamangar F, Dores GM, Anderson WF. 2006. Patterns of cancer incidence, mortality, and prevalence across five continents: Defining priorities to reduce cancer disparities in different geographic regions of the world. J Clin Oncol 24:2137–2150.

Liu J, Ma L, Xu J, Liu C, Zhang J, Chen R, Zhou Y. 2013. Spheroid body-forming cells in the human gastric cancer cell line MKN-45 possess cancer stem cell properties. Int J Oncol 42:453–459.

Micha D, Cummings J, Shoemaker A, Elmore S, Foster K, Greaves M, Ward T, Rosenberg S, Dive C, Simpson K. 2008. Circulating biomarkers of cell death after treatment with the BH-3 mimetic ABT-737 in a preclinical model of small-cell lung cancer. Clin Cancer Res 14:7304–7310.

Nagini S. 2012. Carcinoma of the stomach: A review of epidemiology, pathogenesis, molecular genetics and chemoprevention. World J Gastrointest Oncol 4:156–169.

Olofsson MH, Ueno T, Pan Y, Xu R, Cai F, van der Kuip H, Muerdter TE, Sonnenberg M, Aulitzky WE, Schwarz S, Andersson E, Shoshan MC, Havelka AM, Toi M, Linder S. 2007. Cytokeratin-18 is a useful serum biomarker for early determination of response of breast carcinomas to chemotherapy. Clin Cancer Res 13:3198–3206.

Oyama K, Fushida S, Kinoshita J, Okamoto K, Makino I, Nakamura K, Hayashi H, Inokuchi M, Nakagawara H, Tajima H, Fujita H, Takamura H, Ninomiya I, Kitagawa H, Fujimura T, Ohta T. 2012. Serum cytokeratin 18 as a biomarker for gastric cancer. Clin Exp Med 13(4):289–295.

Petroski MD. 2008. The ubiquitin system, disease, and drug discovery. BMC Biochem 9(Suppl1):S7.

Prabhakaran P, Hassiotou F, Blancafort P, Filgueira L. 2013. Cisplatin induces differentiation of breast cancer cells. Front Oncol 3:134.

Saikawa Y, Fukuda K, Takahashi T, Nakamura R, Takeuchi H, Kitagawa Y. 2010. Gastric carcinogenesis and the cancer stem cell hypothesis. Gastric Cancer 13:11–24.

Scott LC, Evans TR, Cassidy J, Harden S, Paul J, Ullah R, O'Brien V, Brown R. 2009. Cytokeratin 18 in plasma of patients with gastrointestinal adenocarcinoma as a biomarker of tumour response. Br J Cancer 101: 410–417.

She JJ, Zhang PG, Wang X, Che XM, Wang ZM. 2012. Side population cells isolated from KATO III human gastric cancer cell line have cancer stem cell-like characteristics. World J Gastroenterol 18:4610–4617.

Shiozawa Y, Nie B, Pienta KJ, Morgan TM, Taichman RS. 2013. Cancer stem cells and their role in metastasis. Pharmacol Ther 138:285–293.

Signore M, Ricci-Vitiani L, De Maria R. 2011. Targeting apoptosis pathways in cancer stem cells. Cancer Lett 332(2):374–382.

Su L, Xu G, Shen J, Tuo Y, Zhang X, Jia S, Chen Z, Su X. 2010. Anticancer bioactive peptide suppresses human gastric cancer growth through modulation of apoptosis and the cell cycle. Oncol Rep 23:3–9.

Takaishi S, Okumura T, Tu S, Wang SS, Shibata W, Vigneshwaran R, Gordon SA, Shimada Y, Wang TC. 2009. Identification of gastric cancer stem cells using the cell surface marker CD44. Stem Cells 27:1006–1020.

Tan NS, Shaw NS, Vinckenbosch N, Liu P, Yasmin R, Desvergne B, Wahli W, Noy N. 2002. Selective cooperation between fatty acid binding proteins and peroxisome proliferator-activated receptors in regulating transcription. Mol Cell Biol 22:5114–5127.

SUPPORTING INFORMATION

Additional supporting information may be found in the online version of this article at the publisher's web-site.